Enhancement of energy storage in epitaxial PbZrO3 antiferroelectric films using strain engineering

Jun Ge, Denis Remiens, Xianlin Dong, Ying Chen, Jean Costecalde, Feng Gao, Fei Cao, Genshui Wang

Applied Physics Letters

Enhancement of energy storage in epitaxial $PbZrO_3$ antiferroelectric films using strain engineering

Cite as: Appl. Phys. Lett. **105**, 112908 (2014); https://doi.org/10.1063/1.4896156
Submitted: 26 June 2014 • Accepted: 09 September 2014 • Published Online: 18 September 2014

Jun Ge, Denis Remiens, Xianlin Dong, et al.

Enhancement of energy storage in epitaxial $PbZrO_3$ antiferroelectric films using strain engineering

Jun Ge,[1,2] Denis Remiens,[2] Xianlin Dong,[1] Ying Chen,[1] Jean Costecalde,[2] Feng Gao,[1] Fei Cao,[1] and Genshui Wang[1,a)]

[1]*Key Laboratory of Inorganic Functional Materials and Devices, Shanghai Institute of Ceramics, Chinese Academy of Sciences, 1295 Dingxi Road, Shanghai 200050, China*

[2]*IEMN-DOAE-MIMM, CNRS UMR 8520, Université de Valenciennes et du Hainaut Cambrésis, 59313 Valenciennes Cedex 9, Cité scientifique, France and 59655 Villeneuve-d'Ascq Cedex, France*

(Received 26 June 2014; accepted 9 September 2014; published online 18 September 2014)

We demonstrate an approach to enhance the energy storage density W of antiferroelectric film through simple altering a crystallographic orientation of the substrate. We reveal that the antiferroelectric phase stability of $PbZrO_3$ can be enhanced for the (110) or (111) $SrTiO_3$ substrate orientation, thus suppresses the antiferroelectric-ferroelectric phase transition to higher electric field with ~120 kV/cm increment. In addition, the polarization values of these films are also favorably increased hence increases W by 5.3 J/cm^3 at 700 kV/cm. The observed enhancement is found to originate from a high sensitivity of phase transition to mechanical confinements due to the volume expansion at the transition. © *2014 AIP Publishing LLC*.
[http://dx.doi.org/10.1063/1.4896156]

Materials consisted of an ordered array of electric dipoles, but with adjacent dipoles oriented in opposite directions are known as antiferroelectrics (AFEs). The antiparallel dipoles of these compounds can be forced to be parallel by electric fields, corresponding to an electric field-induced AFE-to-ferroelectric (FE) phase transition. Particularly, for perovskite $PbZrO_3$, which is the prototype compound of many AFE materials, the AFE-to-FE phase transition develops a large polarization and volume changes when the applied field E_0 exceeds a critical magnitude E_F. Moreover, the FE phase can turn back to AFE phase when E_0 drops below a critical point E_A. These significant changes at the phase transition present opportunities for potential applications such as in energy storage capacitors and displacement transducers.[1,2] For many of these applications, antiferroelectric materials in the thin film form are required.[3,4]

The properties of thin films can be distinctly different from the intrinsic properties of the bulk counterpart materials because of the enormous strains existing in thin films when one material is deposited on another. Recently, there has been intense research interest in enhancement of particular properties of certain material in thin film form, namely, strain engineering, by elaborate control of substrates and growth parameters. In ferroelectric and multiferroic epitaxy (systems such as $Ba_{1-x}Sr_xO_3$ and $BiFeO_3$), epitaxial strain has been extensively studied and utilized for enhancement of remanent polarization,[5] increase of Curie temperature,[5,6] and modifying the phase diagram.[7,8] In the realm of AFEs, prior work on the effect of compressive strain/stress on bulk AFEs, mainly in $PbZrO_3$ system, has demonstrated a range of novel phenomena such as delayed phase transition,[9] electric field "induced" AFE phase out of FE phase,[10] and enhanced energy density.[11] Hence, it is of highly scientific curiosity and technological significance to clarify the effect of strain on AFE films. Unfortunately, understanding the mechanisms of such effect on AFE film is not well established. Earlier research on $Pb(Zr_{1-x-y}Sn_xTi_y)O_3$ (PZST) films showed tensile strains would make the AFE films prone to the FE phase by observing a "slim loop" double hysteresis.[12,13] However, recent studies argued compressive strain could stabilize a FE phase in $(001)_{pc}$-epitaxial $PbZrO_3$ thin films[14] and multilayer PZST films.[15] Recent theory calculations have suggested that AFE phase stability with strain is also related to the growth orientation of AFE films[16] and has been proven by experimental results from highly oriented polycrystalline $PbZrO_3$ films.[17] Previous studies, however, have focused on how AFE-FE phase transition and related polarization switching are affected by strain. Very little effort has been directed toward deliberate controlling the strain states and the polarization switching properties. Here, we experimentally demonstrate that the E_F and E_A can be greatly elevated in epitaxial $PbZrO_3$ films by changing a crystallographic orientation of the substrate. In addition, the maximum polarization of these films is also favorably increased hence yielding dramatically enhanced energy storage properties of $PbZrO_3$ films.

A series of ~300 nm thick $PbZrO_3$ films were epitaxially grown on (100), (110), and (111) $SrTiO_3$ (STO) substrates at room temperature and 1×10^{-2} mbar of argon by off-axis radio frequency (RF) magnetron sputtering. A ~100 nm thick $LaNiO_3$ (LNO) bottom electrode was firstly deposited at 450 °C and 1×10^{-2} mbar of 20% oxygen and 80% argon via RF magnetron sputtering. The deposited $PbZrO_3$/LNO/STO heterostructures were annealed under air atmosphere at 625 °C for 30 min to crystallize the films into the perovskite phase. The structure and phase purity of the films were checked using Rigaku SmartLab high resolution X-ray diffractometer (HRXRD). The hysteresis loops were performed by aixACCT TF2000FE equipment. The temperature dependence of hysteresis loops was measured in a vacuum of 10^{-5} mbar, increasing the temperature at a ramping rate of 1 K/min.

a)Email: genshuiwang@mail.sic.ac.cn

Figure 1(a) presents the θ-2θ X-ray diffraction (XRD) patterns of the $PbZrO_3$ thin films grown on STO substrates with (100), (110), and (111) orientations. All $PbZrO_3$ films followed the orientation of the substrates and grew in single-phase perovskite structure with no detectable impurity or other phases. The peaks are indexed based on the tetragonal structure. Limited by the accuracy of XRD measurements, we cannot distinguish the (110) peak from (101) peak of $PbZrO_3$ film grown on STO (110) substrate. However, this will not affect our discussion below and our conclusion can be valid for both orientations. Hence, the samples are denoted as PZ(001)/STO, PZ(110)/STO, and PZ(111)/STO. It should be noted that the (002) peak of (001)-oriented thin film demonstrates a weak splitting, which could be induced by formation of a small part of a-domains. The in-plane texturing of $PbZrO_3$ thin films was confirmed by XRD φ scan (Figure 1(b)) of $PbZrO_3$ (110), (100), and (100) reflections of the (001), (110), and (111)-oriented thin films, respectively. The peaks from $PbZrO_3$ films match well with the theoretic assumption, indicating epitaxial growth of all the samples. The smaller lattice constant of bottom electrode LNO ($a = 3.87$ Å) than that of $PbZrO_3$ ($a_{pc} \approx 4.14$ Å) should result in a compressive lattice mismatch. The in-plane strain can be calculated by

$$\varepsilon_{ci} = \left(\frac{c - c_0}{c_0}\right)\left(\frac{u - 1}{2u}\right), \quad (1)$$

where c is the (measured) out-of-plane lattice parameter, c_0 refers to the unstrained out-of-plane lattice parameter from bulk material, and υ is the Poisson ratio (determined to be 0.3[18] from $(Pb_xLa_{1-x})Zr_{0.52}Ti_{0.48}O_3$). Because the film and corresponding substrate have the same growth orientation, we assume that all $PbZrO_3$ films are under similar lattice misfit condition and should receive the same magnitude of strain. Given by Eq. (1), we calculate the in-plane strain ε_{ci} of (001) $PbZrO_3$ film is -0.50%. To further confirm the in-plane compressive strain, the peak of (103) reflection was also measured. (The θ-2θ data are shown in supplementary Figure S1.[19]) Since the (001) peak is already established, the (100) component can be readily extracted. The resulting strain $\varepsilon_{mi} = (a_{film} - a_{bulk})/a_{bulk}$ is -0.55%, which is consistent with the value of strain we calculated from the out-of-plane lattice constant.

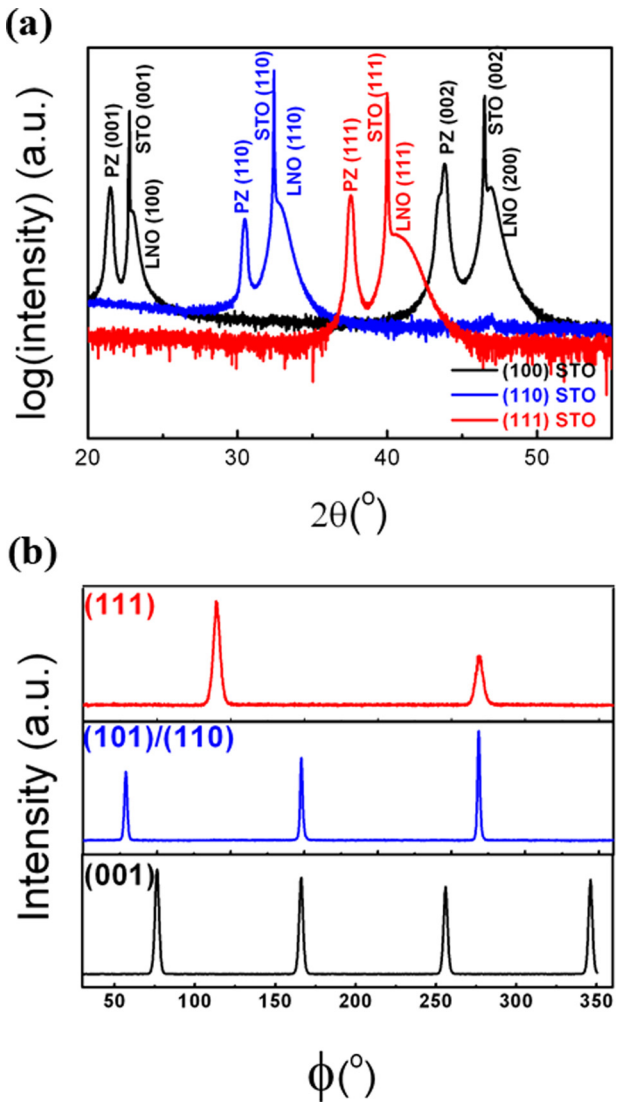

FIG. 1. (a) θ-2θ X-ray diffraction patterns (XRD) of $PbZrO_3$/LNO/(100)STO, $PbZrO_3$/LNO/(110)STO, and $PbZrO_3$/LNO/(111)STO. (b) Patterns of XRD φ scan to confirm the in-plane texture of the $PbZrO_3$ films.

Figure 2 shows the polarization versus electric field (P-E) loops of all the three samples. It can be seen that PZ(001)/STO have a well-developed double hysteresis loops, indicating its AFE nature. Interestingly, PZ(110)/STO and PZ(111)/STO show a mixed antiferroelectric-ferroelectric behavior as suggested by the "triple" hysteresis loop. This phenomenon has recently also been found in high-quality epitaxial $PbZrO_3$ film with (100) orientation.[20] A plausible explanation is the existence of a FE phase along the c-axis with a relatively low spontaneous polarization. Also, PZ(111)/STO has P_{max} slightly higher than PZ(110)/STO, but all possess larger polarization ~45 $\mu C/cm^2$ than ~32 $\mu C/cm^2$ of PZ(001)/STO, as the polar direction is (111) crystallographic direction of the pseudo-cubic perovskite until cell. Finally, PZ(110)/STO and PZ(111)/STO illustrate a remarkable increase in the AFE-FE and FE-AFE switching field compared with PZ(001)/STO. The accurate value of E_F and E_A can be obtained from the switching current peak during

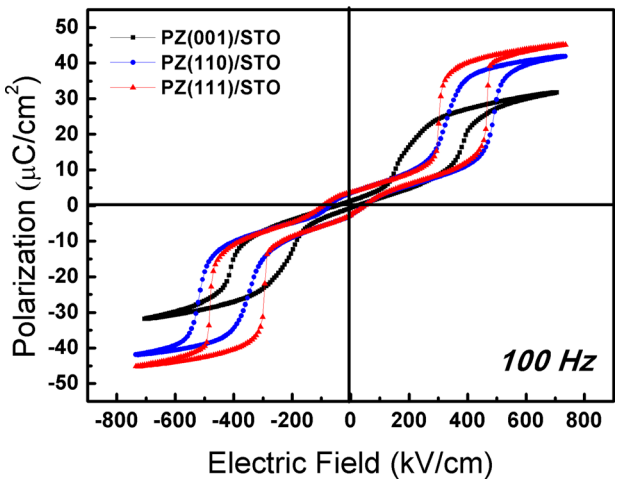

FIG. 2. Room temperature hysteresis loops for PZ(001)/STO, PZ(110)/STO, and PZ(111)/STO.

the *P*-E loops measurements. It is observed that the E_F and E_A are ~500 kV/cm and ~320 kV/cm, respectively, for PZ(111)/STO and ~380 kV/cm and ~200 kV/cm, respectively, for PZ(001)/STO, corresponding to a 120 kV/cm increase. The increase of switching field implies the difference of free energies between two phases is enlarged, and the AFE phase becomes more stable for PZ(110)/STO and PZ(111)/STO.

There exist a few discussions that might be helpful to explain the phenomena we observed here. First, it is believed that the compressive stress can shift the AFE-FE and FE-AFE transition to higher electric field in $PbZrO_3$-based bulk ceramics[9] and even induce a AFE phase out of FE phase in particular situations.[10] This is due to the significant volume expansion during the AFE-FE transition of polycrystalline ceramics. Furthermore, Lillo *et al.* performed density-function calculations[16] on strained $PbZrO_3$ film and found different dependence relationships of AFE phase stability with strain for different growth orientation in a strain region of −1%–1.5%, which can be applied to our films. Here, we explain such phenomena with a clear physical picture and our conclusion is in excellent agreement with the theory calculations.

A schematic of the primitive cells in AFE and FE phases with different orientations is shown in Figure 3, based on the model of Xu *et al.*[12] Figure 3(a) shows the unit cell of $PbZrO_3$ under different electric fields. At zero electric field, the orthorhombic cell of $PbZrO_3$ is a multiple unit cell and contains eight primitive cells, which have a tetragonal structure ($a_0 = \sim 4.16$ Å, $b_0 = \sim 4.16$ Å, $c_0 = \sim 4.11$ Å).[14,21] The polar direction of the antiparallel dipoles is along the [110] direction of the tetragonal primitive cell. When the electric field is high enough to switch the AFE into FE phase, the tetragonal primitive cell becomes rhombohedral with the polar directions along the [111] direction. The lattice angle of the unit cell of the FE rhombohedral phase α_{Rh} is very close to 90° (89.8° or 89.95°), and the lattice parameter a_{Rh} of FE rhombohedral phase is a little smaller than a_{tet} of the AFE tetragonal primitive cell, but obviously larger than c_{tet}. Figure 3(b) shows the primitive cells with (111) orientation in AFE and FE phases. The situation of primitive cells with (110) or (101) orientation would be similar. It can be seen that the films will expand in the plane parallel to the film surface after being switched to the FE phase because a_{Rh} is much larger than c_{tet}. Therefore, the in-plane compressive strain will make the films prone to the AFE phase, thus shifts the E_F and E_A to higher value. However, such kind of delay will not apply for (001) $PbZrO_3$ films. As shown in Figure 3(c), because a_{Rh} is a little smaller than a_{tet}, the films will contract a little bit along the in-plane direction when AFE-FE phase transition occurs; hence, in this case, the compressive stress might stabilize the FE phase instead of the AFE phase.

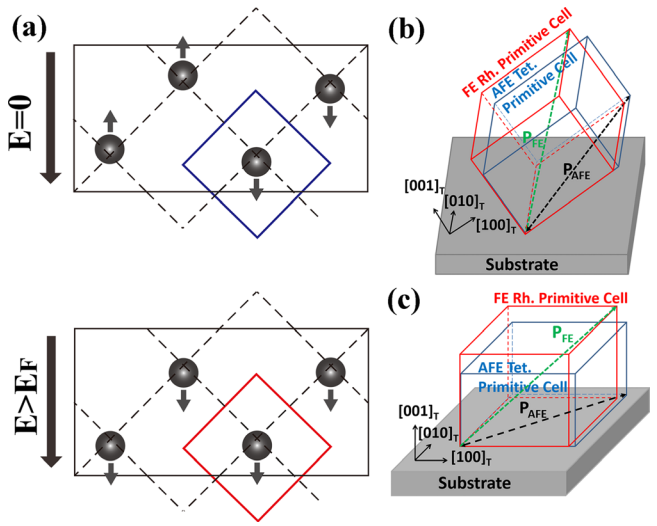

FIG. 3. (a) Projection of the $PbZrO_3$ orthorhombic unit cell onto the ab plane under different electric fields. The antiparallel displacement of Pb^{2+} at zero electric field and forced parallel displacement of Pb^{2+} at electric field higher than E_F was schematically shown. The square containing one Pb^{2+} represents a tetragonal primitive cell (blue line) at zero electric field and a rhombohedral (blue line) at electric field higher than E_F. Three-dimensional schematic diagram of the primitive cells with (b) (111) orientation and (c) (001) orientation in AFE and FE phases.

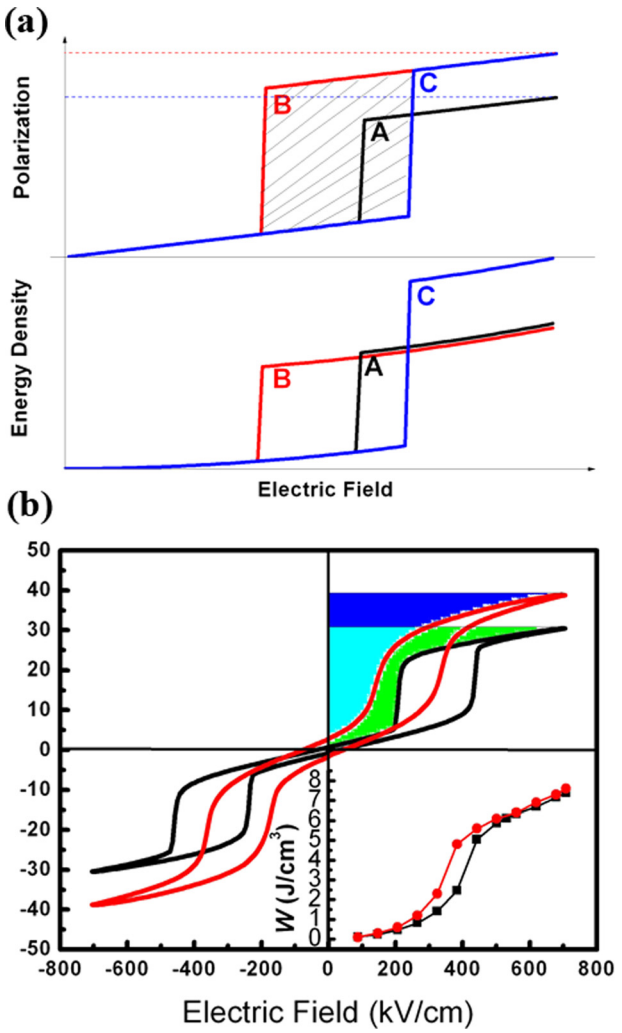

FIG. 4. (a) Fictitious AFE capacitor "A" develops lower saturated polarization than "B" but shows higher phase switching field. Therefore, while "B" develops greater energy density at low fields, the ultimate energy storage capabilities are the same as "A." Curve "C" possesses both high polarization value and large switching field (late polarization saturation); hence, a much higher electric energy density can be achieved. (b) *P*-E loops of $PbZrO_3$ films on SiO_2/Si substrates with (001) and (110)/(101) orientation, respectively. Inset shows the energy density of both two samples with electric field. It can be seen the "jump" of energy density at certain field matches well with the AFE-FE transition field extracted from the hysteresis loops.

The increase of both maximum polarization and transition field could in turn increases the energy density of $PbZrO_3$ film following by

$$W = \int_{P_{max}}^{P_r} EdP \text{ (upon discharging)}, \quad (2)$$

where E is the electric field, P_r and P_{max} are the remanent polarization and polarization at the highest field, respectively. The effect of manipulating the transition field and P_{max} can be seen explicitly by considering the fictitious example illustrated in Figure 4(a). There are three slim-loop polarization-field curves (A, B, and C) along with the energy stored in each as a function of field (calculated according to Eq. (2)). Although "B" has higher P_{max} than "A," the lower transition field restricts it to have the same energy density of "A." In contrast, "C" can store much larger energy than "B" with the benefit of higher transition field.

However, it is worth noting that the high P_{max} and large transition field are usually exclusive in one certain material, which can be explained by that the higher P_{max} means the orientation of film is nearer to polar vector of FE phase hence lead to lower transition field.[22,23] Figure 4(b) shows a typical example to compare (110)/(101)-oriented $PbZrO_3$ film (PZ(110)/Si) with (001)-oriented $PbZrO_3$ film on Si (PZ(001)/Si).[17] The shaded areas represent the recoverable energy density during the FE-AFE switching. The inset plots the curve of energy density of two films with electric field indicating two films have similar value of energy density. By contrast, our epitaxial samples on STOs with certain orientations show promising energy storage density because of their capacity of both high P_{max} and large transition field. The dependence curves of energy density on electric field of all three samples shown in Figure 5 were investigated. With the increasing of electric field, the energy density of all samples first increases slowly and shows an interrupt jump where the phase transition occurs. It is clear that PZ(110)/STO and PZ(111)/STO show a notable enhancement in the energy storage density when compared to PZ(001)/STO sample. At room temperature, the energy density at 700 kV/cm is 7.4 J/cm^3, 12.2 J/cm^3, and 12.5 J/cm^3 for PZ(001)/STO, PZ(110)/STO, and PZ(111)/STO, respectively. Note that in pure $PbZrO_3$ film, 7.4 J/cm^3 is already a pretty high value of energy density compared with other report.[24] It shows that approximately 70% enhancement in energy density can be obtained in PZ(110)/STO and PZ(111)/STO samples compared with PZ(001)/STO, which is not the case between PZ(110)/Si and PZ(001)/Si. In addition, in order to highlight the role of epitaxial strain, we deliberately prepared polycrystalline (110)/(101)-oriented $PbZrO_3$ film on STO substrate (detailed preparation and structure information, supplementary material[19]), denoted as PZ(110)-poly/STO. It can be seen that the PZ(110)-poly/STO shows a rather diffused curve with the energy density of 9.2 J/cm^3 at 700 kV/cm, corresponding to a 24% increase compared with PZ(001)/STO, however, obviously lower than the energy density of PZ(110)/STO. This result strongly indicates that epitaxial strain in our samples is the dominated factor that influences the transition field and energy density of $PbZrO_3$ films.

Devices in practical applications are often needed to operate above room temperature; therefore, the temperature stability of energy density is required. We measured the hysteresis loops from 290 K to 420 K with roughly 15 K between each point. The AFE-FE and FE-AFE switching fields decrease with increasing temperature, corresponding to the thermo-induced AFE to paraelectric transition. The energy density can be plotted versus temperature as shown in Figure 6. It can be seen that the energy density of all samples show a slow decline as temperature increases and they retain at least 70% of their energy density at 420 K. This finding indicates that all samples have rather good temperature stability up to 420 K with the decreasing of energy density well below 0.3% per degree. This indicates that our electroceramic dielectric might have important advantages over the other technologies, which might struggle in high temperature environments. For example, the terpolymer of VDF-TrFE–chlorofluoroethylene, an extensively studied polymer dielectric for energy storage,[25] will melt around 390 K. Besides, it is worth noting that there is still plenty of scope for improving the temperature stability of our film,

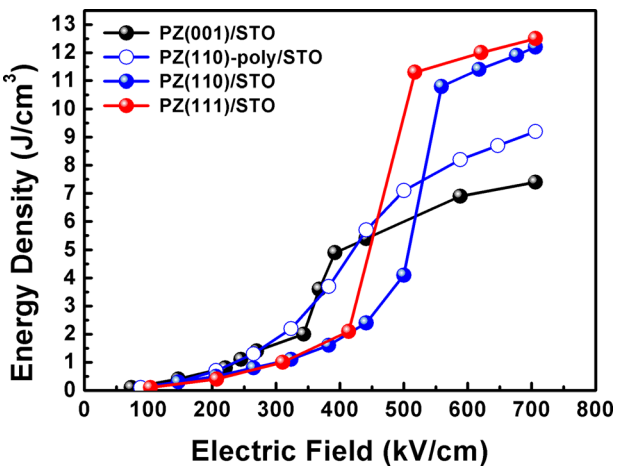

FIG. 5. Dependence of energy density on electric field for PZ(001)/STO, PZ(110)/STO, PZ(110)-poly/STO, and PZ(111)/STO.

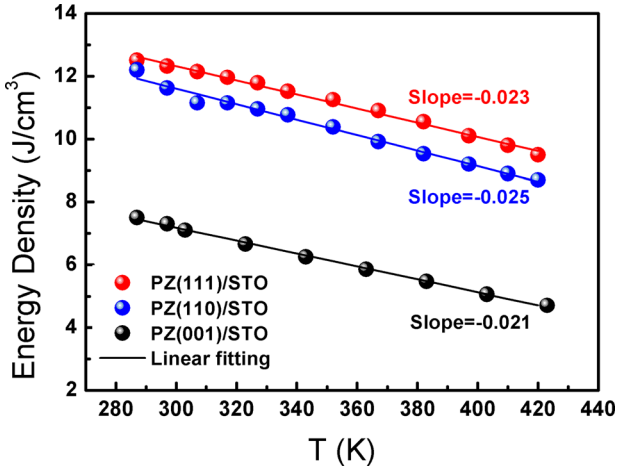

FIG. 6. The temperature dependence of energy density for PZ(001)/STO, PZ(110)/STO, and PZ(111)/STO measured at 700 kV/cm.

such as ion doping like partial substitution Sr^{2+} for Pb^{2+}, which will increase the Curie temperature.[26]

In conclusion, we revealed the effect of strain on polarization switching of epitaxial AFE films with different orientations. Altering the crystallographic orientation of the substrate to (110) or (111) enabled us to change the constrain states of the films and suppress the AFE-FE phase transition to higher electric field. In addition, a larger saturated polarization could also be achieved for the film with (110) or (111) orientation, thereby yielding a dramatically enhanced energy storage density. Furthermore, the energy density showed a good stability with temperature up to 420 K. At last, it is worth mentioning that our demonstrated approach can also be applied to enhance properties for other application. For example, reducing the E_F, which might be achieved by an engineering opposite from here, can be useful for enhanced piezoelectric response. We hope that these findings may open a route to advance studies on $PbZrO_3$-based AFE functional devices.

The authors would like to thank Dr. Yves Sama and Dr. Pascal Roussel for their support for sputtering process and HRXRD measurements, respectively. This work was supported by NSAF (No. U1330128), National important basic research project (No. 2012CB619406), Shanghai International Science and Technology cooperation project (No. 13520700700), Open Project Key Laboratory of Polar Materials and Devices Ministry of Education (Grant No. KFKT20120001), and international partnership project of Chinese Academy of Science.

[1]X. Hao, J. Zhai, L. B. Kong, and Z. Xu, Prog. Mater. Sci. **63**, 1 (2014).
[2]K. Yao, S. Chen, M. Rahimabady, M. S. Mirshekarloo, S. Yu, F. E. Tay, T. Sritharan, and L. Lu, IEEE Trans. Ultrason. Ferroelectr. Freq. Control **58**(9), 1968 (2011).
[3]X. Hao, Z. Yue, J. Xu, S. An, and C.-W. Nan, J. Appl. Phys. **110**(6), 064109 (2011).
[4]M. S. Mirshekarloo, K. Yao, and T. Sritharan, Appl. Phys. Lett. **97**(14), 142902 (2010).
[5]K. J. Choi, M. Biegalski, Y. L. Li, A. Sharan, J. Schubert, R. Uecker, P. Reiche, Y. B. Chen, X. Q. Pan, V. Gopalan, L.-Q. Chen, D. G. Schlom, and C. B. Eom, Science **306**(5698), 1005 (2004).
[6]J. H. Haeni, P. Irvin, W. Chang, R. Uecker, P. Reiche, Y. L. Li, S. Choudhury, W. Tian, M. E. Hawley, B. Craigo, A. K. Tagantsev, X. Q. Pan, S. K. Streiffer, L. Q. Chen, S. W. Kirchoefer, J. Levy, and D. G. Schlom, Nature **430**(7001), 758 (2004).
[7]J. Wang, J. B. Neaton, H. Zheng, V. Nagarajan, S. B. Ogale, B. Liu, D. Viehland, V. Vaithyanathan, D. G. Schlom, U. V. Waghmare, N. A. Spaldin, K. M. Rabe, M. Wuttig, and R. Ramesh, Science **299**(5613), 1719 (2003).
[8]J. H. Lee, P. Murugavel, H. Ryu, D. Lee, J. Y. Jo, J. W. Kim, H. J. Kim, K. H. Kim, Y. Jo, M. H. Jung, Y. H. Oh, Y. W. Kim, J. G. Yoon, J. S. Chung, and T. W. Noh, Adv. Mater. **18**(23), 3125 (2006).
[9]X. Tan, J. Frederick, C. Ma, E. Aulbach, M. Marsilius, W. Hong, T. Granzow, W. Jo, and J. Rödel, Phys. Rev. B **81**(1), 014103 (2010).
[10]X. Tan, J. Frederick, C. Ma, W. Jo, and J. Rodel, Phys. Rev. Lett. **105**(25), 255702 (2010).
[11]S. E. Young, J. Y. Zhang, W. Hong, and X. Tan, J. Appl. Phys. **113**(5), 054101 (2013).
[12]B. M. Xu, Y. H. Ye, and L. E. Cross, J. Appl. Phys. **87**(5), 2507 (2000).
[13]B. M. Xu, X. H. Ye, Q. M. Wang, N. G. Pai, and L. E. Cross, J. Mater. Sci. **35**(23), 6027 (2000).
[14]A. R. Chaudhuri, M. Arredondo, A. Hahnel, A. Morelli, M. Becker, M. Alexe, and I. Vrejoiu, Phys. Rev. B **84**(5), 054112 (2011).
[15]M. S. Mirshekarloo, K. Yao, and T. Sritharan, Adv. Funct. Mater. **22**(19), 4159 (2012).
[16]S. E. Reyes-Lillo and K. M. Rabe, Phys. Rev. B **88**(18), 180102 (2013).
[17]J. Ge, D. Remiens, J. Costecalde, Y. Chen, X. Dong, and G. Wang, Appl. Phys. Lett. **103**(16), 162903 (2013).
[18]B. Ma, S. Liu, S. Tong, M. Narayanan, and U. Balachandran, J. Appl. Phys. **112**(11), 114117 (2012).
[19]See supplementary material at http://dx.doi.org/10.1063/1.4896156 for detailed information of structure property.
[20]L. Pintilie, K. Boldyreva, M. Alexe, and D. Hesse, J. Appl. Phys. **103**(2), 024101 (2008).
[21]E. Sawaguchi, H. Maniwa, and S. Hoshino, Phys. Rev. **83**(5), 1078 (1951).
[22]X. Hao, J. Zhai, J. Yang, H. Ren, and X. Song, Phys. Status Solidi RRL **3**(7–8), 248 (2009).
[23]J. Ge, G. Pan, D. Remiens, Y. Chen, F. Cao, X. Dong, and G. Wang, Appl. Phys. Lett. **101**(11), 112905 (2012).
[24]J. Parui and S. B. Krupanidhi, Appl. Phys. Lett. **92**(19), 192901 (2008).
[25]B. Chu, X. Zhou, K. Ren, B. Neese, M. Lin, Q. Wang, F. Bauer, and Q. M. Zhang, Science **313**(5785), 334 (2006).
[26]X. Hao, J. Zhai, and X. Yao, J. Am. Ceram. Soc. **92**(5), 1133 (2009).